Evolution of the electronic structure of CaO thin films following Mo interdiffusion at high temperature

Yi Cui,[1,*] Yi Pan,[1,†] Leandro Pascua,[1] Hengshan Qiu,[1,‡] Christian Stiehler,[1] Helmut Kuhlenbeck,[1] Niklas Nilius,[2,*] and Hans-Joachim Freund[1]

[1]*Fritz-Haber-Institut der Max-Planck-Gesellschaft, Faradayweg 4–6, D-14195 Berlin, Germany*
[2]*Carl von Ossietzky Universität Oldenburg, Institut für Physik, D-26111 Oldenburg, Germany*

The electronic structure of CaO films of 10–60 monolayer thickness grown on Mo(001) has been investigated with synchrotron-mediated x-ray photoelectron spectroscopy (XPS) and scanning tunneling microscopy (STM). Upon annealing or reducing the thickness of the film, a rigid shift of the CaO bands to lower energy is revealed. This evolution is explained with a temperature-induced diffusion of Mo ions from the metal substrate to the oxide and their accumulation in the interface region of the film. The Mo substitutes divalent Ca species in the rocksalt lattice and is able to release electrons to the system. The subsequent changes in the Mo oxidation state have been followed with high-resolution XPS measurements. While near-interface Mo transfers extra electrons back to the substrate, generating an interface dipole that gives rise to the observed band shift, near-surface species are able to exchange electrons with adsorbates bound to the oxide surface. For example, exposure of O_2 results in the formation of superoxo species on the oxide surface, as revealed from STM measurements. Mo interdiffusion is therefore responsible for the pronounced donor character of the initially inert oxide, and largely modifies its adsorption and reactivity behavior.

PACS number(s): 73.40.Ns, 73.61.Ng, 68.37.Ef, 68.35.Dv

I. INTRODUCTION

The physical and chemical properties of a given material are inseparably connected to its electronic behavior. This is evident for semiconductors, where doping is used to engineer the band structure and therewith the carrier concentration, electron mobility, and luminescence properties [1]. A well-known example from chemistry concerns heterogeneous catalysis [2,3]. Many chemical reactions rely on redox processes, i.e., on the exchange of electrons between the active surface and the reactants. The ability of a catalyst to accept or donate charges is naturally given by its electronic structure. Whereas metal particles are able to exchange electrons over a wide energy range, the electronic structure of oxides is often governed by band gaps and thus is incompatible with the requirement of a high redox activity. Catalytically active supports might still be fabricated on the basis of reducible oxides, such as ceria [4] or zirconia [5], or by preparing nonreducible oxides with high defect concentrations [6]. The latter route has the disadvantage that surface defects tend to heal at the high pressures and temperatures used in chemical reactions, resulting in a continuous degradation of the catalytic activity [7]. Stable and durable redox centers might be formed by inserting aliovalent impurities into an oxide matrix, whose charge state differs from the one of the host ions [2,8]. Whereas doping with low-valence ions produces acceptor states in the oxide band gap, high-valence dopants give rise to excess electrons that might be transferred to adsorbates on the catalyst surface.

As recently demonstrated, traces of high-valence Mo incorporated into a CaO matrix drastically affect the growth behavior of electronegative metals and the adsorption and activation of molecules, e.g., O_2, on the oxide surface [9,10,11]. In both case, the excess electrons from the Mo dopants were made responsible for the enhanced activity of the originally inert material. In this paper, we study the electronic consequences of embedding aliovalent Mo ions into the rocksalt lattice. We follow the alteration of the oxide electronic structure as a function of the dopant concentration, the preparation conditions, and the thickness of the oxide film. The electronic properties are monitored with high-resolution photoelectron spectroscopy, carried out with synchrotron radiation, and conductance spectroscopy performed with a scanning tunneling microscope (STM). While the first technique allows us to probe the core levels of dopants and parent ions, the latter provides spatially resolved insight into the electronic structure of the oxide surface. Our experiments reveal that the CaO bands shift to more negative energies with increasing doping level, being a unique fingerprint of a rising Fermi level in the oxide band gap. Moreover, we provide evidence that charge-transfer reactions between dopants and adsorbates on the oxide surface have a beneficial effect on the reactivity of the oxide material.

II. EXPERIMENT

High-resolution x-ray photoelectron spectroscopy (XPS) data were acquired with synchrotron radiation from the UE52-PGM beamline of the BESSY II electron storage ring in Berlin, using a Scienta R4000 hemispherical electron energy analyzer. To optimize the surface sensitivity of the measurements, the energy of the x rays was chosen such that the photoelectrons of interest had a kinetic energy of ∼100 eV. The STM experiments were carried out with a custom-built ultrahigh-vacuum setup operated at liquid helium temperature (10 K).

---

*Corresponding authors: yicui@fhi-berlin.mpg.de, niklas.nilius@uni-oldenburg.de

†Present address: Paul-Drude-Institut für Festkörperelektronik, Hausvogteiplatz 5–7, 10117 Berlin, Germany.

‡Present address: Xinjiang Technical Institute of Physics and Chemistry of CAS, 830011 Urumqi, China.

The CaO films were prepared by Ca deposition onto a Mo(001) single crystal in 5×10^{-7} mbar of O_2, followed by vacuum annealing to stimulate film crystallization [12]. Most of the samples were actually fabricated with a two-step procedure. First, a seed film of 10–20 monolayer (ML) thickness was grown by reactive Ca deposition and 1000 K annealing, while this layer was thickened in a second step by additional Ca-O deposition and annealing to temperatures between 700 and 1100 K. The following philosophy lies behind this two-step approach. CaO films are known to be affected by self-doping, which proceeds via Mo diffusion from the metal support to the oxide lattice [13]. In order to control the Mo concentration, either the annealing temperature, hence the driving force for diffusion, or the film thickness needs to be varied. The two-step scheme now allows us to alter the Mo content in the chemically relevant surface region of the oxide without corrupting its crystallographic quality that mainly depends on the annealing conditions. Hereby, the first, high-temperature step generates a crystalline, but Mo-rich, template, on which the subsequent layers can develop with high quality already at moderate temperature. With this approach, we have successfully varied the Mo concentration from 0 to $\sim 10^{14}$ cm^{-2} in a near-surface region. As both STM and XPS are only sensitive to the topmost 20 ML, the presence of a Mo-rich interface oxide appears to be irrelevant for our conclusions. We want to stress that, as a result of the two-step preparation, the Mo doping level is not homogenous across the film but reduces when approaching the surface.

III. RESULTS and DISCUSSION

A. Temperature-dependent topographic and electronic properties of CaO films

Figure 1 displays a series of STM images of CaO(001) films prepared with increasing temperature in the second annealing step. Already at 700 K, orthogonal steps are discernable on
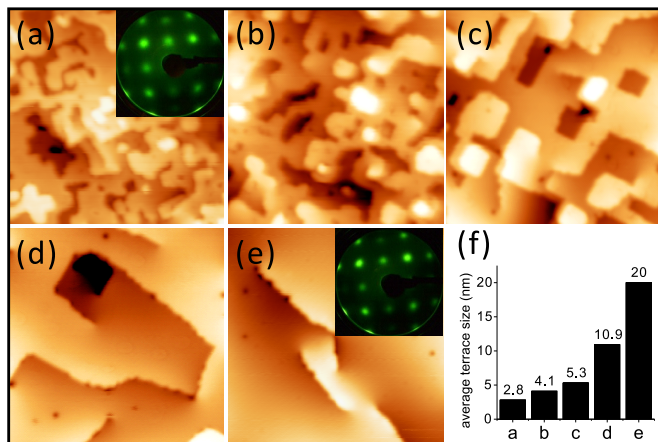

FIG. 1. (Color online) STM images (40×40 nm^2) of 40 ML CaO grown with the two-step procedure and annealed to final temperatures of (a) 700 K (6.0 V, 50 pA), (b) 800 K (5.0 V, 50 pA), (c) 900 K (4.5 V, 30 pA), (d) 1000 K (4.0 V, 50 pA), and (e) 1100 K (3.8 V, 50 pA). The insets show LEED patterns taken with 170 eV electron energy. (f) Diagram of the average terrace size on CaO films as deduced from (a)–(e).
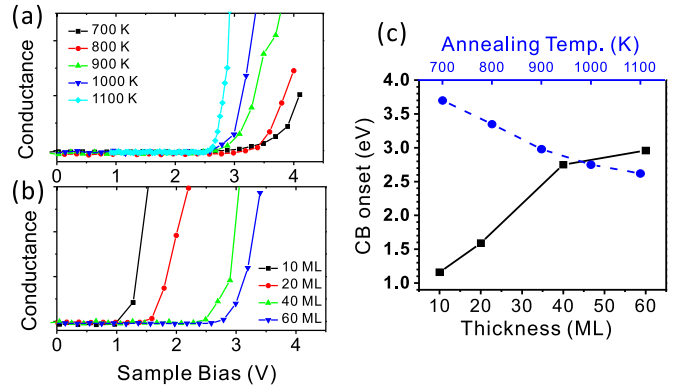

FIG. 2. (Color online) (a) STM dI/dV spectra showing the conduction band onset of a 40 ML thick CaO film as a function of the final annealing temperature. (b) Shift of the conduction band edge when increasing the film thickness from 10 to 60 ML. The annealing temperature was kept constant at 1000 K in all cases. (c) Evolution of the conduction band onset with film thickness (black solid line) and annealing temperature (blue dashed line).

the surface, providing a clear indication for the development of crystalline CaO(001) patches delimited by nonpolar and energetically preferred [100] edges [14]. A distinct, square pattern in low-energy electron diffraction (LEED), as shown in the inset of Fig. 1(a), confirms the good crystallographic order, even of the moderately annealed oxide films. An increase of the annealing temperature mainly leads to the development of larger CaO(001) terraces that are not only separated by step edges, but also by oxide dislocation lines. The CaO dislocation network compensates for misfit strain with the Mo(001) support and for lateral strain between adjacent oxide domains in out-of-phase registry [15]. With increasing temperature, the density of the screw and edge dislocations gradually decreases and the oxide surface becomes atomically flat over large distances. The evolution of terrace sizes as a function of temperature is summarized in Fig. 1(f), but can be qualitatively deduced also from the sharper LEED pattern shown in the inset of Fig. 1(e).

Electronically, CaO is governed by a 7.1 eV band gap [16], and no tunneling current can be detected at negative polarity or positive voltages below the conduction band (CB) onset. Electron transport through thick CaO films is therefore feasible only in a narrow bias window between the CB onset and the field-emission resonances around the vacuum energy. A first hint for changes in the CaO electronic structure with temperature comes from the analysis of the sample bias that can be used for imaging the differently prepared oxide films (Fig. 1). The accessible range gradually shifts to lower voltages when raising the annealing temperature (6.0 → 3.8 V), indicating a downshift of the CB onset. This trend is reproduced in direct measurements of the band onset via tunneling spectroscopy, in which the conductivity onset decreases almost linearly with the maximum annealing temperature [Fig. 2(a)]. We note that the temperature effect is most pronounced for an intermediate film thickness (20–30 ML) and fades away for thicker films. Conversely, the band onset can be tuned by varying the film thickness and keeping the annealing temperature constant at 1000 K. This trend is
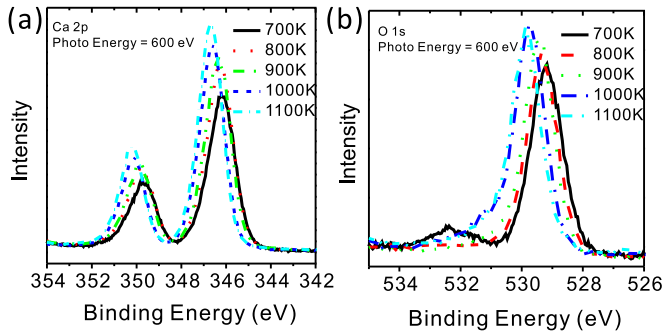
FIG. 3. (Color online) XP-spectra of (a) the Ca $2p$ and (b) the O $1s$ core levels in a 40 ML thick CaO film after annealing to the indicated temperatures. The excitation energy of the x-ray photons was set to 600 eV.
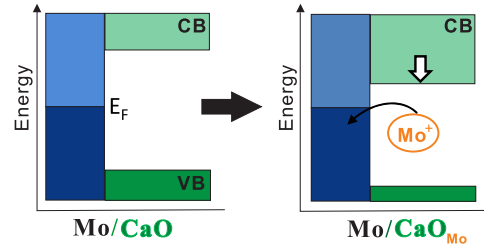

FIG. 4. (Color online) Energy diagram connecting the charge transfer from Mo dopants to the support with the formation of an interface dipole and a subsequent band shift. The latter was monitored with STM conductance and XP spectroscopy.

depicted in Fig. 2(b), which exhibits a continuous upshift of the CB onset when increasing the vertical extension of the film from 10 to 60 ML.

The evolution of the CaO electronic structure with either annealing temperature or film thickness is not only observed in STM conductance measurements, but can be detected with x-ray photoelectron spectroscopy as well. XPS is a powerful technique to follow global changes in the surface electronic structure. High surface sensitivity is hereby achieved by irradiating the sample at grazing incidence or by using small kinetic energies of the emitted photoelectrons. In contrast to STM measurements, the focus of the experiment is now on the low-lying core levels and not on the valence states at the Fermi level. Nonetheless, XP and tunneling spectra reveal similar shifts in the electronic states, in particular, if those are caused by electrostatic effects, e.g., band bending in response to excess surface charges, and not by chemical bonding. In this case, shifts in the core-level binding energies (BEs) can be directly compared to changes in the oxide valence and conduction band. The position of the Ca $2p$ and O $1s$ core levels across an annealing series is displayed for a 40 ML CaO film in Figs. 3(a) and 3(b). Both data sets show an identical increase in BE by 0.7 eV when raising the temperature from 700 to 1100 K. This value compares well with the 1.0 eV shift deduced from STM conductance spectra. The discrepancy reflects the fundamental differences in both methods; while dI/dV spectroscopy probes the local properties of ideal CaO regions, XPS is an integral technique that averages over surface defects and irregularities. Besides their energy shift, the core-level peaks also become narrower and more intense in well-annealed films, indicating a higher crystallinity of the oxide lattice.

The downshift of the CB edge with stronger annealing or a reduced thickness of the film can be consistently explained by the impact of Mo ions that diffuse into the CaO lattice during preparation. The Mo ions substitute Ca^{2+} species and serve as high-valence dopants in the rocksalt lattice, as they are able to adopt higher oxidation states between +3 and +5 [8]. In an ideal bulk environment, the extra electrons remain trapped at the Mo sites, as the empty Ca $3s$ conduction states are too high in energy to be populated at finite temperature. In thin films, on the other hand, charge transfer may occur either to the metal substrate beneath or to adsorbates on the

oxide surface. The electron flow from Mo substitutional ions to the support generates an interface dipole that lowers the vacuum energy in the film and shifts the oxide electronic states to more negative energies [17]. The observed downshift of the CB edge with increasing annealing temperature thus provides evidence for an interdiffusion of Mo donors into the film, followed by a charge backdonation to the support (Fig. 4). The upshift with increasing film thickness, on the other hand, is caused by the progressive screening of this interface dipole combined with the inability of near-surface Mo ions to transfer electrons back to the metal. Using a simple plate capacitor model $\Delta U = \frac{\sigma d}{\varepsilon_0 \varepsilon_r}$, we may determine the total number of transfer electrons from the experimental CB shift of 1.0 eV when annealing a 40 ML film to 1100 K. For a rough picture, we have set the mean distance between ionized Mo species and metal support to $d = 4.8$ nm (20 ML) and used a CaO dielectric constant of $\varepsilon_r = 10$ [16]. The resulting charge density amounts to 0.018 C/m^2, which corresponds to $\sim 1 \times 10^{13}$ Mo^{3+} ions per cm^2. Note that this model is necessarily simplified as the Mo density is not homogenous across the CaO film [18].

B. Evolution of the Mo core-level spectra during CaO annealing

To elucidate how the charge state of the Mo dopants changes upon annealing and how this alters the global electronic structure of the CaO film, we will next focus on the Mo core levels. Their BE position with respect to the Ca and O states also helps to differentiate between band-bending effects and changes in the chemical environment and stoichiometry of the film upon annealing. For this purpose, the photoelectron signal of metallic Mo, being exclusively located in the support, is used as an internal reference. Figure 5(a) display a series of Mo $3d$ spectra, measured on a 40 ML thick CaO film during a temperature ramp from 700 to 1100 K. In all spectra, the characteristic Mo^0 doublet with a low-energy shoulder at 277.7 eV is detected as a unique signature of the metallic support [19]. In addition, features with higher BE emerge in the XP data, indicating the formation of oxidized Mo ions upon annealing. The intensity and less pronounced the position of these peaks vary in a characteristic manner with the thermal treatment. The first doublet at 228.5 eV, labeled with (a) in Fig. 5(a), appears at 900 K and gradually intensifies during annealing. Based on tabulated BE values [19], this feature is assigned to weakly oxidized Mo^{2+} or Mo^{3+} species. Simultaneously, a high-energy doublet, denoted with (c),
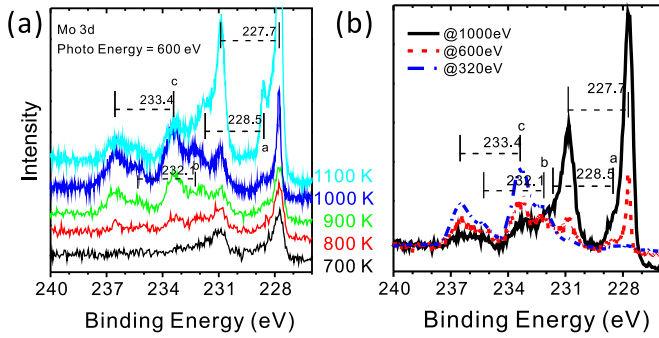
FIG. 5. (Color online) (a) XP spectra of Mo $3d$ core levels in a 40 ML thick, doped CaO film, measured as a function of the annealing temperature. (b) XP spectra of Mo $3d$ core levels measured with variable photon energy for a 40 ML thick CaO film annealed to 1000 K. The surface sensitivity of the measurement increases with lower excitation energy.

FIG. 6. (Color online) STM images ($40 \times 27 \, \text{nm}^2$) of one and the same Mo sample after depositing 40 ML CaO and annealing to 1000 K. While in (a), a highly stepped region is shown that is barely covered with oxide, a flat and homogenous CaO film is visible in (b). (c) Sketch of an inhomogeneous CaO/Mo sample that would account for the Mo core level spectra measured in this study. (d) STM image ($100 \times 100 \, \text{nm}^2$) of 40 ML CaO after a final annealing step to 1100 K, showing an extended dewetting region.

shows up at 233.4 eV and develops the largest intensity of all Mo features upon annealing. It has been matched to fully oxidized Mo^{6+}, although its BE is somewhat higher than the literature value of 232.7 eV [20]. The difference would be in line with the band-bending effect that has been identified previously for the Ca and O BE values (Fig. 3). A third spectral feature, labeled with (b), is detected at an intermediated BE of 232.1 eV, but develops only weak intensity. When accounting for the band-bending effect again, it may be ascribed to Mo^{5+} species.

All spectra in Fig. 5(a) have been measured with 600 eV excitation energy, which corresponds to an inelastic mean free path of $\sim$8 Å for the Mo $3d$ electrons, and puts the source of the photoelectrons into the three topmost oxide planes [21]. To take advantage of the synchrotron radiation, different photon energies have been used to vary the information depth of our measurements. The corresponding Mo $3d$ spectra, measured with 1000, 600, and 320 eV photon energy, are depicted in Fig. 5(b). As the energetic photoelectrons easily penetrate the oxide film, the signal of metallic Mo increases substantially with excitation energy. The fingerprint of oxidized Mo ions, on the other hand, is strongest at low photon energies, suggesting that those species are localized in a near-surface region of the oxide. Especially, the highly oxidized Mo^{5+} and Mo^{6+} species are almost exclusively found at the film surface.

Our Mo $3d$ spectra are not fully consistent with results of the STM measurements shown in Fig. 1 for the following reasons. The fingerprint of metallic Mo should be entirely invisible for a homogenous CaO film of 40 ML nominal thickness, given the short inelastic mean free path of the photoelectrons. The observation of a rather pronounced Mo^0 peak and its intensity rise upon annealing indicates a patched nature of the oxide film, in which the Mo(001) support is exposed in certain regions of the sample. We assign those CaO-free areas to step bunches on the Mo single crystal that were indeed found in the STM images [Fig. 6(a)]. On these densely stepped regions, no oxide film is stabilized and Mo^0 photoelectrons are easily released. Naturally, the STM images have been taken on flat regions, covered with a thick CaO layer, and are therefore not in contradiction to the XPS data. An example of the
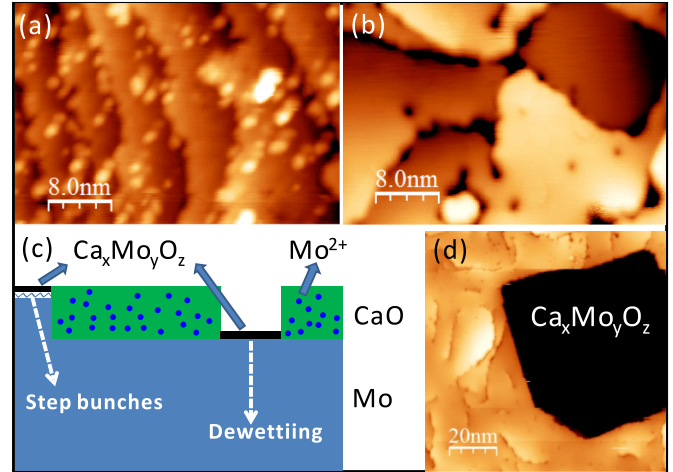
inhomogeneity of our sample is given in Figs. 6(a) and 6(b), which display a stepped and a fully oxidized surface in close spatial vicinity.

The patched character of the CaO film intensifies upon annealing, as the oxide dewets from the substrate at high temperature [Fig. 6(d)]. As a result, the weight of uncovered metal increases and highly oxidized Mo^{5+} and Mo^{6+} ions become abundant in the XP spectra. The Mo dopants in the film, on the other hand, are expected to maintain a $+2$ or $+3$ oxidation state, as the excess electrons find no empty state inside the oxide band gap. This conclusion has been corroborated by several earlier experiments that shall be summarized here [8]. First, Mo-doped CaO features a pronounced donor character, which leads to the formation of negatively charged Au atoms and to the activation of O_2 molecules towards superoxo oxygen upon adsorption [9,10]. The required charge transfer is possible only for Mo ions that have not yet reached their highest oxidation state, while Mo^{5+} and Mo^{6+} species are unsuitable donors [22,23]. In addition, the Mo impurities have been visualized directly as circular features in STM images of the CaO surface [18]. The ring structures were associated with charging events in the tip-electric field, in which the Mo dopants temporarily lose electrons to the CaO conduction band. Again, this phenomenon is restricted to Mo^{2+} and Mo^{3+} species and does not occur for ions in a higher oxidation state. Moderately charged Mo species with a high redox potential in the CaO lattice are best represented by the doublet at 228.5 eV in our XP spectra [feature (a)]. We note that a $+2$ charge state in general is untypical for Mo and can be explained only when taking the specific electronic environment of Mo ions inside the rocksalt lattice into account.

In conclusion, the specific Mo core-level spectra presented here provide evidence for a spatially inhomogeneous CaO film,

as sketched in Fig. 6(c). A large portion of the Mo signal hereby results from CaO-free sample regions, in which metallic as well as mixed-oxide structures are abundant. The Mo ions inside the oxide matrix, on the other hand, contribute only weakly to the detected spectra. This interpretation is in line with the small number of electronically active Mo species ($\sim 10^{13}$ cm^{-2}) that would be sufficient to produce the band shifts revealed in the experiment. The discrepancy between STM and XPS results thus emphasizes the sometimes conflicting views of global and local experimental techniques onto a given problem.

C. Interplay between electronic structure and adsorption behavior of Mo-doped CaO films

The change in the CaO electronic structure due to Mo interdiffusion, in particular, the shift of the oxide CB towards the Fermi level, has direct consequences on the adsorption behavior of the film. Previous results have indicated that a Mo-doped CaO film has donor character and provides excess electrons to be transferred into adsorbates with high electron affinity [9,10]. As the oxide electronic structure has been monitored here, we can now prove this correlation for the example of O_2 adsorption. Figure 7(a) shows an STM topographic image of the CaO surface after exposure to 10 L O_2 at 20 K. The molecular species are easily discernible as circular depressions on the surface. Using such data sets, the O_2 adsorption probability can be correlated with the energy position of the oxide CB, as probed with tunneling spectroscopy [Fig. 7(b)]. The diagram shows a clear, almost linear relationship, in which a high density of O_2 molecules on the surface corresponds to a low-lying CB onset. Note that only oxygen species that have received an extra electron from a nearby Mo donor are able to bind to the CaO surface, while no adsorption takes place on the nondoped and chemically inert material. Two conclusions can be drawn from this relationship. As the energy of the CB provides an inverse measure of the Mo content in the CaO lattice, it proves that the Mo ions are indeed required to activate and stabilize the O_2 molecules. Moreover, a good energy match between the Mo donor states in the oxide gap and the O_2 affinity level does not seem to be crucial for the charge transfer. In fact, the electron transfer occurs especially

in the case of a low-lying CB, which shifts the Mo donor states to a lower energy as well. Still, the relevant Mo states are above the O_2 affinity level, and charge transfer is not restricted from an energetic point of view, at least for the electron-rich Mo^{2+} and Mo^{3+} species. The limits in the oxygen activation are rather set by the total number of Mo ions in the oxide lattice, their mean separation from the surface, and their charge state. Note that the latter is largely controlled by the presence of parasitic electron traps in the film, such as the metal-oxide interface and electron-accepting point or line defects [24,25]. As electron transfer into the O_2 molecules was found to be efficient, the structural quality of our CaO layers is apparently high enough to maintain the donor character of the oxide [8].

IV. CONCLUSION

Using a combination of x-ray photoelectron and tunneling spectroscopy, we have shown that the electronic states of a CaO thin film can be continuously shifted with respect to the Fermi level of the metal substrate below. The band shift is caused by Mo interdiffusion from the support to the rocksalt lattice, generating electron-rich donor states in the CaO matrix. The Mo ions close to the interface are hereby able to donate electrons back to the support, generating an interface dipole that lowers the vacuum energy and hence the position of the oxide bands. Impurities in a near-surface region, on the other hand, act as charge donors for adsorbates, and are therefore of decisive importance for the adsorption and activation of molecules (O_2, CO_2) and the growth of metal particles.

Our work provides an instructive example that experimental data that have been acquired either with global or local techniques are always susceptible to misinterpretations. Already, tiny uncovered areas in a thick CaO overlayer ($<5\%$) turned out to be sufficient to produce rather dominant Mo signals in the XP spectra, arising either from bare metallic or highly oxidized species present in mixed-oxide phases. None of these parasitic Mo ions are responsible for the donor properties of the doped CaO film, which requires the presence of Mo^{2+} and Mo^{3+} species with a high redox potential. However, these chemically relevant Mo ions showed up only with small intensity in our spectra, a fact that reflects the genuine nature of dopants—to become active already in tiny quantities. In this light, careful sample preparation and a combination of local and nonlocal techniques appear to be crucial to obtain a comprehensive picture of the physics and chemistry of doped oxide materials.
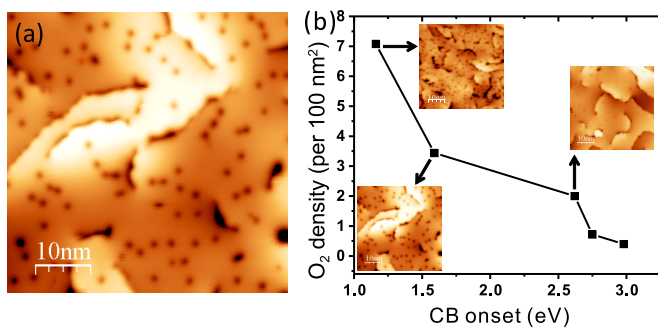

FIG. 7. (Color online) (a) STM topographic image of a 20 ML thick CaO film after exposure to 10 L of oxygen at 20 K. (b) Correlation between the density of O_2 molecules on the CaO surface and the onset of the oxide CB edge as deduced from STM conductance spectroscopy. All STM images in the inset are 50×50 nm^2.

[1] E. F. Schubert, *Doping in III-V Semiconductors* (Cambridge University Press, Cambridge, U.K., 1993), Vol. 27.

[2] W. D. Mross, Catal. Rev. **25**, 591 (1983).

[3] E. W. McFarland and H. Metiu, Chem. Rev. **113**, 4391 (2013).

[4] A. Trovarelli and P. Fornasiero, *Catalysis by Ceria and Related Materials*, Catalytic Science Series, 2nd ed. (World Scientific, Singapore, 2013).

[5] X.-M. Liu, G. Q. Lu, and Z.-F. Yan, Appl. Catal. A: Gen. **279**, 241 (2005).

[6] B. Yoon, H. Häkkinen, U. Landman, A. S. Wörz, J.-M. Antonietti, S. Abbet, K. Judai, and U. Heiz, Science **307**, 403 (2005).

[7] S. Arndt, G. Laugel, S. Levchenko, R. Horn, M. Baerns, M. Scheffler, R. Schlögl, and R. Schomäcker, Catal. Rev.: Sci. Eng. **53**, 424 (2011).

[8] F. Stavale, X. Shao, N. Nilius, H. J. Freund, S. Prada, L. Giordano, and G. Pacchioni, J. Am. Chem. Soc. **134**, 11380 (2012).

[9] X. Shao, S. Prada, L. Giordano, G. Pacchioni, N. Nilius, and H. J. Freund, Angew. Chem. Int. Ed. **50**, 11525 (2011).

[10] Y. Cui, X. Shao, M. Baldofski, J. Sauer, N. Nilius, and H.-J. Freund, Angew. Chem. Int. Ed. **52**, 11385 (2013).

[11] Y. Cui, K. Huang, N. Nilius, and H.-J. Freund, Faraday. Discuss. **162**, 153 (2013).

[12] X. Shao, P. Myrach, N. Nilius, and H. J. Freund, J. Phys. Chem. C **115**, 8784 (2011).

[13] X. Shao, N. Nilius, P. Myrach, H.-J. Freund, U. Martinez, S. Prada, L. Giordano, and G. Pacchioni, Phys. Rev. B **83**, 245407 (2011).

[14] S. Schintke and W.-D. Schneider, J. Phys.: Condens. Matter **16**, R49 (2004).

[15] S. Benedetti, P. Torelli, S. Valeri, H. M. Benia, N. Nilius, and G. Renaud, Phys. Rev. B **78**, 195411 (2008).

[16] R. C. Whited, C. J. Flaten, and W. C. Walker, Solid State Commun. **13**, 1903 (1973).

[17] L. Giordano, F. Cinquini, and G. Pacchioni, Phys. Rev. B **73**, 045414 (2006).

[18] Y. Cui, N. Nilius, H.-J. Freund, S. Prada, L. Giordano, and G. Pacchioni, Phys. Rev. B **88**, 205421 (2013).

[19] C. D. Wagner and G. E. Muilenberg, *Handbook of X-Ray Photoelectron Spectroscopy: A Reference Book of Standard Data For Use in X-Ray Photoelectron Spectroscopy* (Physical Electronics Division, Perkin-Elmer Corporation, Eden Prairie, MN, 1979).

[20] F. Werfel and E. Minni, J. Phys. C: Solid State Phys. **16**, 6091 (1983).

[21] C. J. Powell and A. Jablonski, J. Phys. Chem. Ref. Data **28**, 19 (1999).

[22] J. Andersin, J. Nevalaita, K. Honkala, and H. Hakkinen, Angew. Chem. Int. Ed. **52**, 1424 (2013).

[23] S. Prada, L. Giordano, and G. Pacchioni, J. Phys. Chem. C **117**, 9943 (2013).

[24] H.-M. Benia, P. Myrach, A. Gonchar, T. Risse, N. Nilius, and H.-J. Freund, Phys. Rev. B **81**, 241415 (2010).

[25] K. P. McKenna and A. L. Shluger, Nat. Mater. **7**, 859 (2008).